JOURNAL OF SPACECRAFT AND ROCKETS
Vol. 34, No. 5, September–October 1997

Validation Database for Propulsion Computational Fluid Dynamics

Houshang B. Ebrahimi*
Sverdrup Technology, Inc., Arnold Air Force Base, Tennessee 37389

Validation of computational fluid dynamic (CFD) models appropriate for subsonic through hypersonic flow applications requires careful consideration of the physical processes encountered in these flight regimes and detailed comparisons of the calculated results with experimental data sets that include these processes. The work reported involved two efforts: 1) identification of quality data sets for establishment of a standard validation database and 2) direct comparison of the CFD model results with the measurement database. Three Navier–Stokes-based CFD models were selected for comparison: the three-dimensional, upwind-differenced, finite volume flow solver; the generalized implicit flow solver; and the general aerodynamic simulation program. Computed flow properties from these three models were compared to experimental data from seven selected databases. These databases include measurements from the following experiments: 1) supersonic flow over a rearward-facing step, 2) supersonic, two-dimensional nozzle flow, 3) low subsonic, reacting nozzle flow, 4) combustion in two-dimensional, supersonic flow with tangential hydrogen injection, 5) shear-layer combustion in a supersonic concentric hydrogen/air flow, 6) hypersonic flow over a biconic model with perpendicular nitrogen injection, and 7) sonic, normal injection of staged N_2 jets behind a rearward-facing step into a Mach number 2 airstream. The results of the study indicate that all three models compared reasonably well with flow measurements from the seven validation cases.

Introduction

RECENT interest in hypersonic, airbreathing, single-stage-to-orbit vehicles, such as those being studied by the NASA Hypersonic Research Program, has revealed a requirement for increased understanding of such vehicles. Because of the high Mach numbers and high enthalpies present in hypersonic flight, it is not technically or economically feasible to simulate all conditions of the flight envelope in a ground test facility. Therefore, an increased emphasis is being placed on computational fluid dynamics (CFD) to predict and analyze these types of flowfields and to extend the ground test simulations to desired conditions outside the test matrix. The use of CFD requires a careful strategy to ensure that the computational models are appropriate for the physical phenomena dominating the flight regime and that the models are applied in a timely and efficient manner. Thus, CFD models are often applied along two parallel, coupled paths: one incorporates existing CFD models directly into the design and data analysis process, whereas the other determines the range of validity of the models and identifies improvements needed in the existing model's physical and numerical methodologies. Computational methods, when complemented and coordinated with experimental methods, provide information for designing the experimental setup and selecting the optimum instrumentation for a test. CFD methods can also complement analyses of measured data by carefully simulating the measured results, thus providing computed information beyond what was measured and providing insight into the physical phenomenology contributing to the measured data set. Such coordinated efforts facilitate computational model improvements and enhance data analysis.

Traditional aerodynamic design methodology couples boundary-layer approximate methods with inviscid flow solutions to calculate forces, heat transfer loads, and overall propulsion vehicle performance. For supersonic and hypersonic flight conditions, such an approach may not be suitable due to the presence of strong inviscid/viscous coupling, shock wave/boundary-layer interactions, flow nonuniformities, divergence losses, shear losses, dissociation/recombination chemistry effects, and plume/afterbody interactions.[1–3] In a more-detailed, design-level analysis, parabolized Navier–Stokes (PNS) space-marching techniques are applied to both the inviscid outer flow and the viscous inner flow. Although such methods are not applicable to subsonic flow or separation regions, they are ideal design simulation tools for supersonic flow regimes due to their efficiency.

In the process of selecting and validating CFD models, it is necessary to identify experimental data sets appropriate for evaluation of the physical approximations included in the models. Detailed comparison of the calculated results with data sets provides insight and directs code enhancements to improve the physics included in the computational model and, consequently, the accuracy of the calculations. Improved physical models may be required to properly account for the effects of nonideal gas working fluids, finite rate chemical kinetics, and turbulence/transition models.

In this study, existing computer models capable of solving the Reynolds-averaged Navier–Stokes equations for chemically reacting flows[4,5] were assessed with respect to five categories: 1) development state, 2) adequacy of physical models for flow regimes extending from low subsonic through hypersonic conditions, 3) adequacy of numerical method, 4) model generality, and 5) overall performance of the model with respect to user friendliness, computational resources, and numerical stability. Using these criteria, three CFD models, specifically, the three-dimensional, upwind-differenced, finite volume flow solver (TUFF), the general aerodynamic simulation program (GASP) version 3, and the generalized implicit flow solver (GIFS), were selected for evaluation and validation against seven data sets: 1) supersonic flow over a rearward-facing step, 2) supersonic, two-dimensional nozzle flow, 3) low subsonic, reacting nozzle flow, 4) combustion in two-dimensional, supersonic flow with tangential hydrogen injection, 5) shear-layer combustion in a supersonic concentric hydrogen/air flow, 6) hypersonic flow over a biconic model with perpendicular nitrogen injection, and 7) sonic, normal injection of staged N_2 jets behind a rearward-facing step into a Mach number 2 airstream.

The TUFF code was developed at NASA Ames Research Center for a unified nose-to-tail numerical prediction of three-dimensional flows.[6] It contains chemical models for solving equilibrium, frozen, or finite rate reaction equations. It solves the thin-layer, Navier–Stokes equations and has a two-equation turbulence model, as well as the algebraic Baldwin–Lomax model.

GASP, a three-dimensional, finite volume flow solver, is based on the Roe or Van Leer upwind scheme. GASP solves the integral form of the governing equations, including the full Reynolds-averaged Navier–Stokes, thin-layer, parabolized or Euler equations.[7] GASP contains a generalized chemistry model. The numerical methods

Received Feb. 6, 1995; revision received June 7, 1997; accepted for publication June 22, 1997.

*Senior Engineer, Computational Fluid Dynamics Branch, Technology Department, Arnold Engineering Development Center Group.

employed in GASP are not drastically different from those used in the TUFF code, but GASP has a variety of options, is further developed, and is more efficient.

The GIFS model solves the Reynolds-averaged Navier–Stokes equations using the MacCormack implicit, finite volume algorithm with Gauss–Seidel line relaxation.[8] The GIFS model includes a generalized chemistry model, a Lagrangian particulate model for treating solid or liquid particles, and a two-equation turbulence model. The original objective of the GIFS model development was to provide a flowfield simulation capability that could be used in conjunction with radiative transfer models to predict the radiometric emissions from three-dimensional, multiple-exhaust, plume flowfield interactions emanating from multiple nozzle propulsion vehicles. The Van Leer flux-splitting option has been implemented into the existing GIFS model and provides a more robust solution capability, compared to the original version of the code. Details of the GIFS modification can be found in Ref. 9.

Model Validation

Before using any CFD model in a design or analysis environment, it is necessary to establish confidence in the results obtained from the model. This is accomplished by performing a series of validation exercises, where the results of the calculations are compared with well-characterized experimental data. The objective of the validation is to determine the accuracy of the physical and numerical approximations included in the models and to determine whether model modifications are needed to improve the reliability of the calculated results or to improve the numerical efficiency of the calculation method. Validation not only guards against source coding errors but also provides estimates of the effect of numerical parameters on the computed solution.

Several steps have been identified to assist in the validation and verification of complex CFD models. These steps can be described as follows: 1) defining the critical performance parameter information and primary physical phenomenologies affecting these parameters and establishing the corresponding CFD modeling requirements; 2) establishing the appropriate governing equations and the corresponding physical modeling requirements; 3) identifying and acquiring appropriate, well-characterized benchmark data to establish a standardized database to validate computer models; 4) performing computations for the exact experimental conditions and determining the model sensitivity to the numerical and modeling assumptions; and 5) documenting the validation effort results to the extent necessary to provide other CFD model users with knowledge of the model's capabilities, including the overall accuracy of the calculated results and the sensitivity of the solution to internal parameters such as numerical damping and computational grid refinement.

Validation Database

The flow properties for the seven experiments included in the validation database were simulated by each of the three CFD models. The results of the simulations were compared with flowfield measurements. Each validation experiment was selected to focus on specific physical aspects included in the computational models, starting with the simplest physics and progressing to complex three-dimensional, chemically reacting cases. First, two-dimensional supersonic flow over a rearward-facing step was simulated by all three CFD models and compared with the corresponding validation measurements to evaluate specific turbulence models. Second, each CFD model was applied to simulate two-dimensional scramjet nozzle flow to assess its accuracy for predicting measured pressures and nozzle divergence losses. Third, the case involved was axisymmetric, subsonic nozzle flow with axial injection of hydrogen. These conditions were simulated and compared with measurements to assess the chemical kinetics approximations included in each CFD model. Fourth, an axisymmetric scramjet combustor with coaxial hydrogen injection was simulated and compared with corresponding measurements to assess the hydrogen combustion model and ignition prediction. Fifth, the case included two-dimensional tangential fuel injection. Both the fourth and fifth cases focus on turbulent mixing and chemical kinetics. The sixth and seventh test cases represented complex flow environments. These cases included a three-dimensional biconic geometry and a rearward-facing step. Both of these cases have normal injection of nitrogen into a primary airstream. These two cases were selected to assess three-dimensional flow effects, including the extent of injectant penetration into the primary flow stream, and the size, location, and characteristic flow properties of the separation zone resulting from the normal injection. The numerical analysis of the biconic geometry and the rearward-facing step cases with normal injection are the most challenging for CFD simulation and will provide valuable insight into real-world CFD applications for simulation of propulsion combustion phenomena. The experiments used for validation of the CFD models are summarized in Table 1.

Boundary Condition and Computational Setup

In this study an attempt was made to utilize the same or similar physical and numerical models in all three codes. For all GASP and GIFS calculations, the Van Leer flux-splitting options were utilized. However, for the TUFF solutions, flux-difference splitting with Roe's approximate Riemann solver was used. The third-order, upwind inviscid flux option of Van Leer with the min–mod limiter based on pressure and species densities was used for the GASP code. Both GIFS and TUFF were run with second-order spatial accuracy. Implicit schemes were used in all three codes. Turbulence calculations with the GIFS and TUFF codes were obtained using a κ–ε model, whereas calculations using the GASP code were obtained using the modified Cebeci and Smith turbulence model as described in Ref. 2.

The grids used for the flow simulations of the experimental database were identical for all three CFD codes. In this study, at least 10 grid points were placed between the wall and the location corresponding to $y+ = 80$, and the first grid point was located no farther from the wall than $y+ = 4$. The grid was refined in the shear-layer region separating the airstream and fuel stream to capture the gradient in this region. A grid refinement study also was performed. The results of this study indicate that a finer grid did not change the results significantly. The initial flowfield profiles were uniform for all test cases except for the two-dimensional combustor case at Mach number 2.44 and were obtained from the experimental data. No-slip wall boundary conditions were used at all solid surfaces, as well as adiabatic conditions for the cases where the surface temperature was not specified in the data set. Noncatalytic wall boundary conditions were assumed. The same starting time step and the same ending time step were used for all three codes, corresponding to a CFL number of 0.2 and 4, respectively. Calculations were run until a reduction of four orders of magnitude in the solution residual was obtained, after which mass, momentum, and energy were

Table 1 Experimental database conditions and related issues

Experiment	No. of cases	Freestream Mach number	Chemistry	Items of interest	CPU, H[a] INDIGO 2
Smith[10] two-dimensional rearward step	2	2.5, 3.5	Perfect gas	Separation and wall pressure	T = 7, G = 1.4, GF = 2.9
Hopkins et al.[11] two-dimensional nozzle	4	1.65	Perfect gas	Wall pressure external interaction	T = 2.8, G = 0.6 GF = 1.1
Henry–Beach[13] axisymmetric nozzle	1	1.9	H_2–air	Ignition mixing	T = 33, G = 9, GF = 16
Kent–Bilger[12] subsonic nozzle	1	0.043	H_2–air	Ignition mixing	G = 39, GF = 17
Burrows–Kurkov[14] two-dimensional combustor	1	2.44	H_2–air	Ignition mixing	T = 26, G = 9, GF = 14.1
Prats–Metzger[17] three-dimensional case	2	9.7	Perfect gas	Wall pressure and separation	T = 169, G = 68, GF = 96
McDaniel et al.[18] three-dimensional combustor	2	2.06	Perfect gas	Penetration and separation	T = 209, G = 94, GF = 124

[a]T = TUFF, G = GASP, and GF = GIFS.

reasonably conserved to ensure convergence. Inasmuch as all three codes contain a general chemistry model, the same reaction sets and the same number of species were used for all codes. The species and reactions being considered are

$$OH + O = H + O_2 \qquad OH + H = H_2 + O$$

$$OH + OH = H_2O + O \qquad OH + H_2 = H_2O + H$$

$$H + H + M = H_2 + M \qquad H + O + M = OH + M$$

$$O + O + M = O_2 + M \qquad H + OH + M = H_2O + M$$

$$H + O_2 + M = HO_2 + M$$

Supersonic Flow over a Rearward-Facing Step

The TUFF, GASP, and GIFS models were validated against data collected from two rearward-facing step experimental conditions involving a perfect gas (air) working fluid. The rearward-facing step experiment provides a fundamental test case to evaluate CFD simulations of the expansion fan region between the freestream flow and the reattachment shock, the compression effect of the shock, and the relatively constant pressure region between the reattachment shock and the shear layer. The geometry for the two test cases that were selected is shown in Fig. 1. The freestream Mach numbers were 2.5 ($Re = 4.6 \times 10^5$/in.) and 3.5 ($Re = 4.3 \times 10^5$/in.), respectively. The rearward-facing step height was 0.443 in. in each case. At these conditions the flow should be laminar with transition to turbulent flow taking place in the shear layer downstream of the step. An 85 × 78 computational grid was used for each solution.

The surface static pressure distribution predicted by the flow solvers is shown in Fig. 2 for the Mach number 2.5 case along with the experimental pressure measurements.[10] The results for the Mach number 3.5 cases are shown in Fig. 3. All codes predict the surface pressures within the scatter of the experimental data. The shock reattachment length simulated by the TUFF, GASP, and GIFS models is in reasonable agreement with the experimental data for both Mach number conditions.

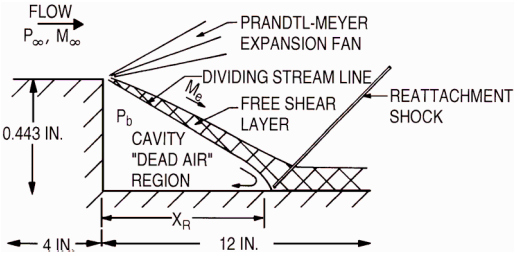

Fig. 1 Rearward-facing step problem geometry and flowfield description.

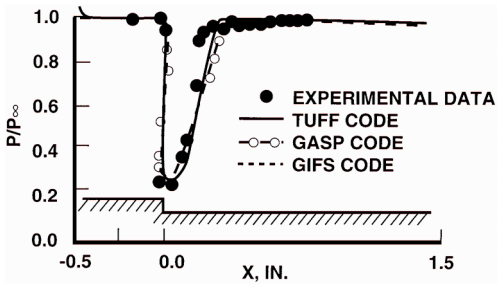

Fig. 2 Comparison of the surface pressure distribution (M_∞ = 2.5).

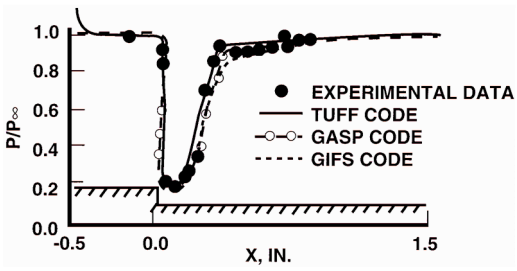

Fig. 3 Comparison of the surface pressure distribution (M_∞ = 3.5).

Supersonic Nozzle Validation Results

The modeling of supersonic nozzle flowfields is complex due to flow nonuniformities and inherent performance losses that occur in convergent/divergent nozzles. The loss mechanisms include nozzle divergence, wall-shear effects, dissociation/recombination chemistry effects, and plume/afterbody interactions. Before confidence can be placed in a CFD model to predict the chemistry and three-dimensional effects of supersonic nozzle flowfields, the computational model first must be evaluated in an aerodynamic sense, showing accuracy in predicting the pressure and nozzle divergence losses.

To validate CFD models for simulating supersonic nozzle flow phenomena involving a perfect gas working fluid, existing experimental data[11] were utilized. The measurement database was collected from four separate nozzle experiments, two with aft bodies parallel to the nozzle centerline (0-deg afterbody) and the others with the aft body inclined at an angle of 20 deg to the nozzle centerline (20-deg afterbody). The geometries and operating conditions are shown in Fig. 4. The computational grid utilized 100 radial points and 150 axial points.

Surface static pressure measurements obtained along the nozzle aftbody are presented for all four cases in Figs. 5 and 6. The calculated results from the TUFF, GASP, and GIFS models are also included for direct comparison. The pressures, measured and calculated, are normalized by the local initial freestream static pressure P_∞. The computational results all assumed identical uniform combustor exit conditions as the nozzle entrance conditions and compared favorably with the experimental data for all four experiments

Subsonic Nozzle Reacting Case

The GASP and GIFS models were applied to simulate combustion in a subsonic shear layer created by the axial injection of hydrogen into a coflowing stream of air. The measurements were collected by Kent and Bilger.[12] The geometry and flow conditions are shown in Fig. 7. Unlike the two preceding cases, the Mach number was subsonic in both the injectant and the primary streams. Figure 8 compares computed and measured centerline axial profiles of H_2 and H_2O mole fractions and static temperature from the injection point to an axial position equal to 140 injection jet diameters downstream. Figure 9 presents comparisons of the computed and measured radial profiles of H_2, O_2, and H_2O mole fractions at a downstream axial location equal to 120 jet radii downstream of the injection point. The solutions were obtained assuming eight chemical species (H_2, N_2, O_2, OH, H_2O, O, H, and HO_2) and nine chemical reactions in the kinetic chemistry models. Initially, the GASP model produced an unstable solution at these conditions because of the low Mach number and numerical model selected by this user. A very low CFL number and initialization of the GASP solution using the GIFS flowfield were required to ultimately obtain a stable GASP solution. The computational grid used consisted of 72 grid points in the radial direction and 76 grid points in the axial direction.

Supersonic Hydrogen–Air Validation

The three CFD models were applied to simulate combustion in a supersonic shear layer created by coaxial hydrogen injection into a supersonic air freestream. The experimental data in this case were reported by Henry and Beach.[13] The geometry and flow conditions are shown in Fig. 10. Cold hydrogen (T = 251 K) at Mach number 2.0 was injected concentrically into a supersonic, Mach 1.9 stream of hot vitiated air (T = 1495 K). Figure 11 compares TUFF, GASP, and GIFS radial profile predictions of N_2, O_2, and H_2O mass fractions with experimental profile data obtained at an axial location equal to 27.9 jet diameters downstream of the injection point. Because the N_2 is contained solely in the airstream and the H_2O mass fraction is a product of combustion of the two streams, these profiles are an indicator of the turbulent mixing in the shear layer and the degree of chemical reaction that has occurred. Comparisons of the data and computed values are in reasonable agreement. The computational grid utilized 70 points radially and 90 points axially.

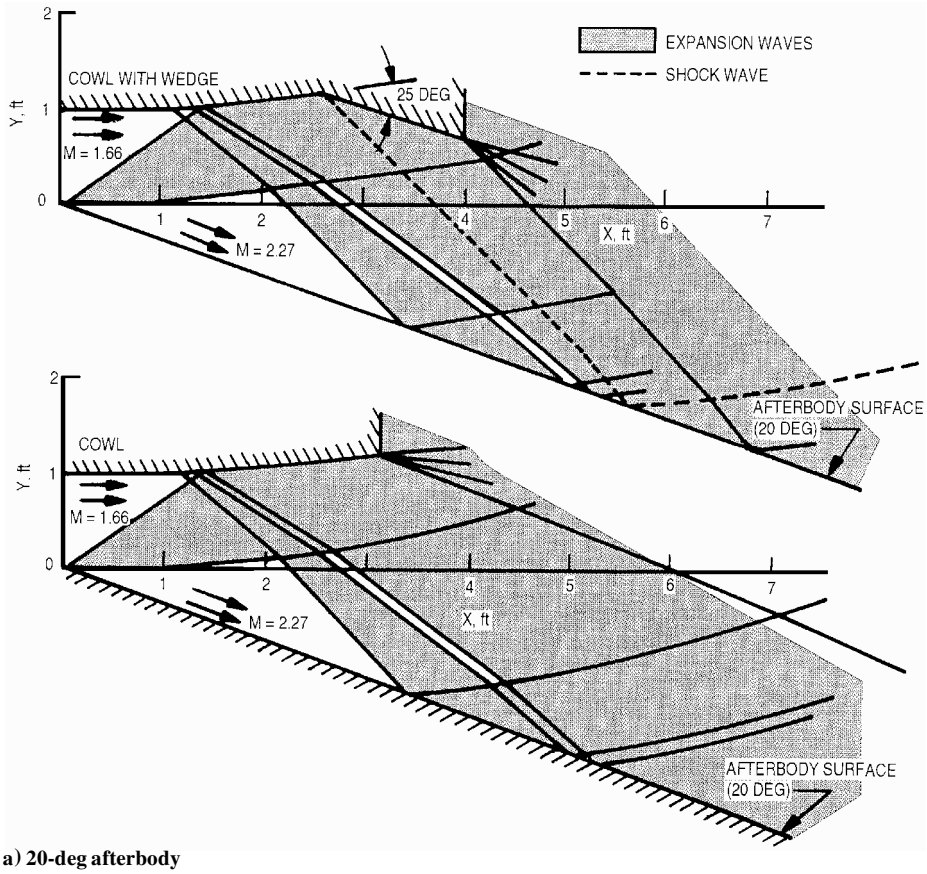

a) 20-deg afterbody

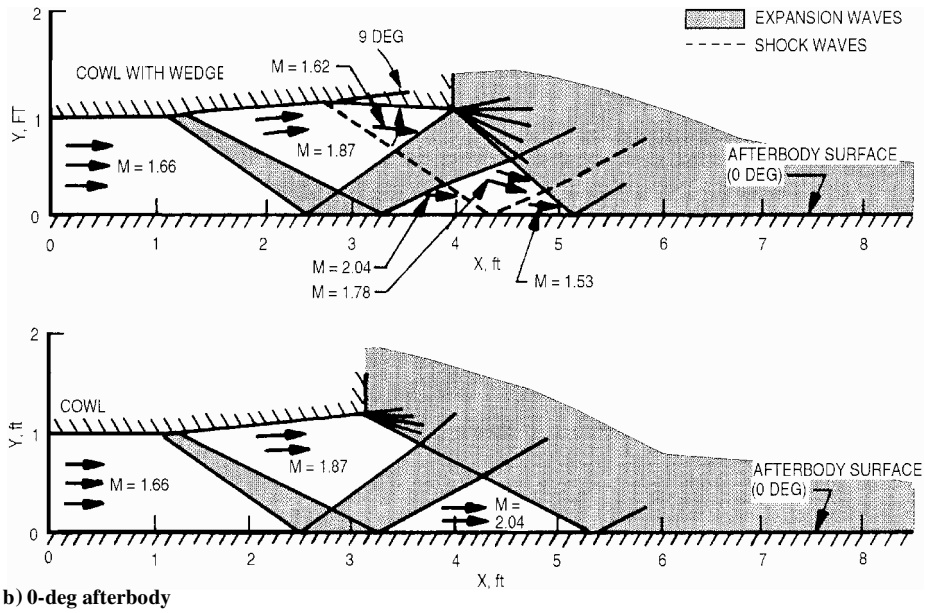

b) 0-deg afterbody

Fig. 4 Two-dimensional case. Nozzel entrance conditions: $M = 1.657$, $T = 4091°$R, $U = 5206.4$ ft/s, and $P = 4298$ psf. Freestream conditions: $M = 6.0$, $T = 348°$R, $U = 5488.6$ ft/s, and $P = 58.04$ psf.

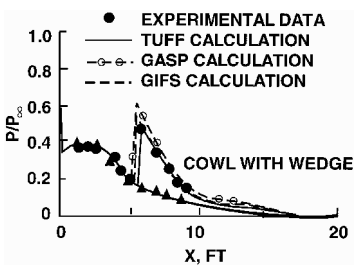

Fig. 5 Comparison of the surface pressure distribution, 20-deg afterbody.

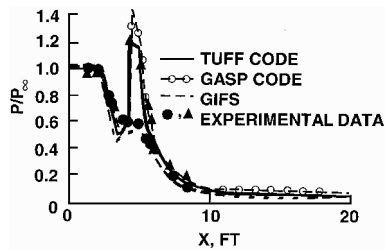

Fig. 6 Comparison of the surface pressure distribution, 0-deg afterbody.

Hydrogen–Air Validation

The TUFF, GASP, and GIFS models were applied to simulate combustion in a supersonic shear layer with tangential hydrogen injection at the wall.[14] This test case is among the few sets of data that provide detailed measurements of the initial conditions required to computationally simulate the problem properly. The geometry and operating conditions are shown in Fig. 12. In this case, a sonic jet of hydrogen is injected tangentially near the wall into a Mach 2.44 vitiated airstream flowing in a duct with diverging walls. The wall temperature was held fixed at 298 K. The inlet boundary conditions were obtained from experimental data. The incoming airstream had a thick boundary layer approximately three times the diameter of the initial H_2 jet. The jet-slot height was 0.4 cm. The thermal boundary layer was approximately twice the jet height.

The author previously applied a two-dimensional, PNS model[1] to simulate this experiment, using the measured initial conditions. This solution produced reasonable agreement with the measurements. However, this case has also been modeled by several other investigators, reporting poor agreement with the experimental data.[7,15] The reason for the poor agreement appears to be that the calculations were obtained assuming uniform flow as the inflow boundary

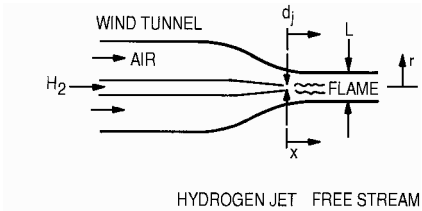

	HYDROGEN JET	FREE STREAM
MACH NUMBER, M	0.0135	0.043
TEMPERATURE, T, K	300	300
VELOCITY, u, m/s	17	15.1
PRESSURE, p, MPa	0.1	0.1
MASS FRACTION:		
a_{H_2}	1.0	0
a_{O_2}	0	0.232
a_{N_2}	0	0.768
a_{H_2O}	0	0

Fig. 7 Experimental apparatus and flow condition for the axisymmetric subsonic combustor: $L = 0.3054$ m, $d_j = 0.00762$ m, and injector lip thickness = 0.00020 m.

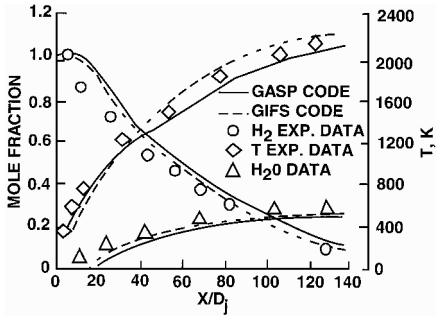

Fig. 8 Comparison of axial temperature, H_2O and H_2 concentration distribution on centerline.

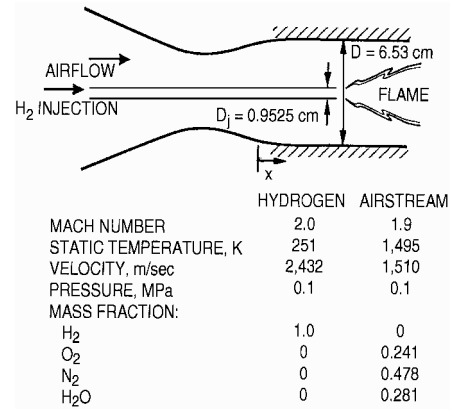

	HYDROGEN	AIRSTREAM
MACH NUMBER	2.0	1.9
STATIC TEMPERATURE, K	251	1,495
VELOCITY, m/sec	2,432	1,510
PRESSURE, MPa	0.1	0.1
MASS FRACTION:		
H_2	1.0	0
O_2	0	0.241
N_2	0	0.478
H_2O	0	0.281

Fig. 10 Experimental apparatus flow conditions for the axisymmetric combustor.

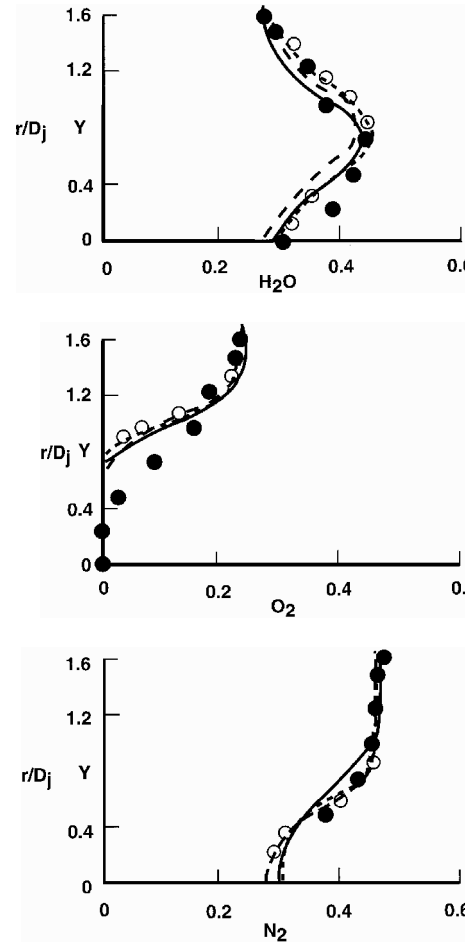

Fig. 11 Comparison of mass fraction profiles: – – –, GIFS; ○, GASP calculation; ——, TUFF calculation; and ●, experimental data.

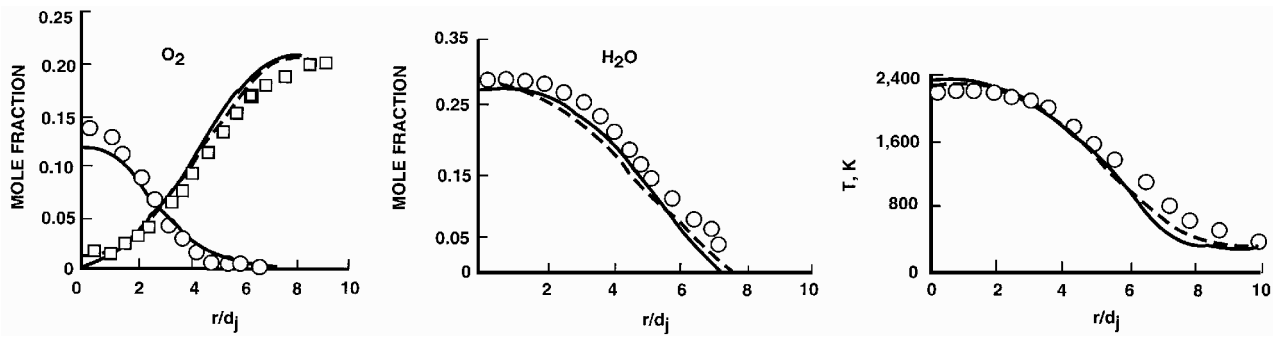

Fig. 9 Comparison of mole fraction and temperature radial profiles at $X/D_j = 120$: ○, H_2; □, O_2; ——, GASP calculation; and – – –, GIFS.

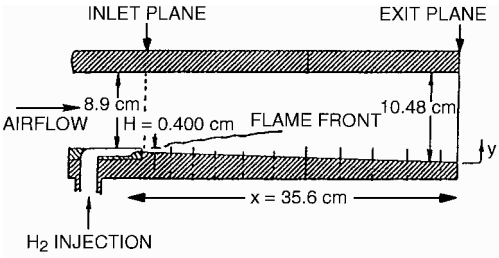

	HYDROGEN JET	AIR STREAM
MACH NUMBER	1.0	2.44
TEMPERATURE, K	254	1270
VELOCITY, m/sec	1216	1764
PRESSURE, MPa	0.1	0.1
MASS FRACTION:		
H_2	1.00	0
O_2	0	0.258
N_2	0	0.486
H_2O	0	0.256

Fig. 12 Burrows and Kurkov[14] model configuration and operating conditions.

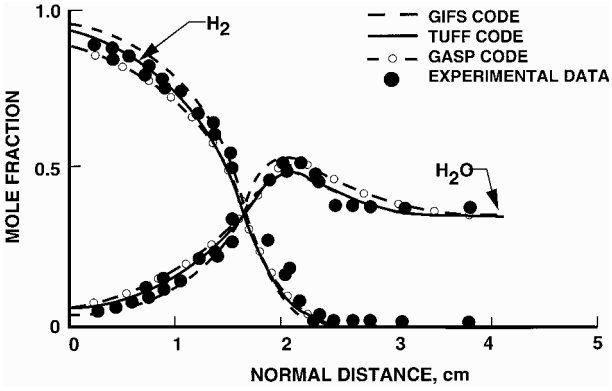

Fig. 13 Comparison of predicted mole fraction profiles with experimental data at $x = 35.6$ cm.

condition instead of using the measured inflow conditions as was done in the current study. A detailed description of a procedure for determining the initial turbulence quantities is given in Refs. 1 and 4.

Calculated chemical species profiles for H_2 and H_2O at 35.6 cm downstream of the injection point were obtained assuming eight chemical kinetic reactions and nine chemical species in the model. The calculated profiles are compared with the experimental data in Fig. 13. The overall agreement is quite reasonable, and the flame position, indicated by the location of the maximum H_2O mass fraction, is accurately predicted. The computational grid consisted of 70 points in the radial direction and 76 points in the axial direction.

These results along with the unfavorable comparison by other investigators indicate that the solution is extremely sensitive to the initial profiles used in a flow solver. This conclusion was also substantiated in a previous study by the author evaluating the initial profile effect on the scramjet combustor and nozzle performance.[16] This study also indicates that the determination of the initial turbulence quantities based on the velocity and density profiles is required to properly analyze the flowfield.

Jet Interaction

The test case selected for this validation is airflow over a biconic geometry with normal injection of nitrogen.[17] The leading cone half-angle of the biconic geometry is 10.4 deg, while the trailing cone half-angle is 6 deg. The geometry is schematically shown in Fig. 14. A lateral jet stream is located 0.455 m aft of the biconic nose. The centerline of the jet is oriented normal to the cone centerline in the vertical plane. The biconic geometry has a 0-deg angle of attack with respect to the freestream flow. The freestream Mach number is 9.7, with a corresponding static temperature of 61 K and density of 0.025 kg/m^3. The jet fluid is nitrogen and is injected vertically at

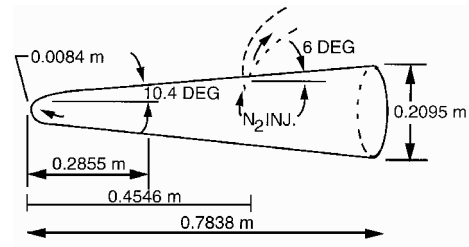

TEST CONDITIONS	FREE STREAM	NITROGEN
PRESSURE, Pa	523	10,000
DENSITY, Kg/m^3	0.025	2.2
MACH NO.	9.7	2.0

Fig. 14 Biconic test model.

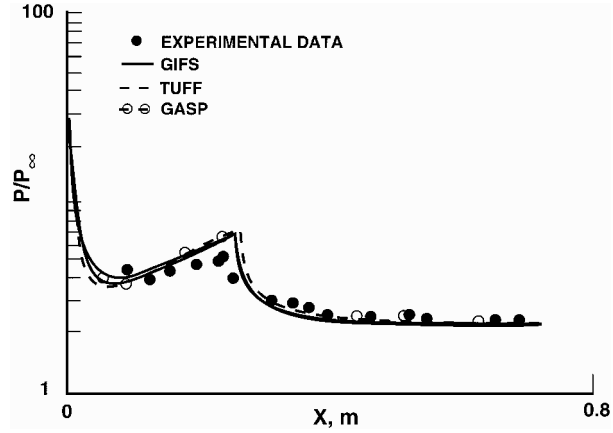

Fig. 15 Comparison of the surface pressure distribution without injection.

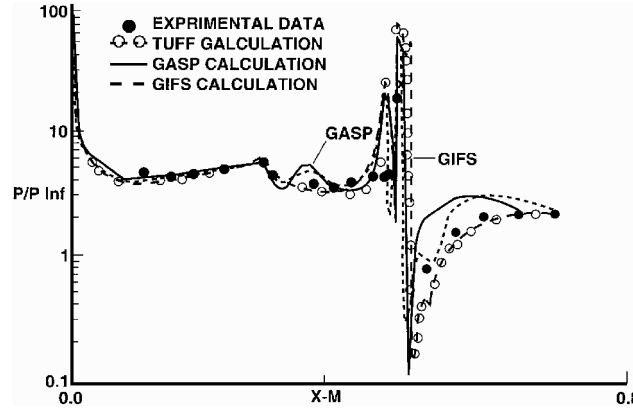

Fig. 16 Comparison of the surface pressure distribution with injection.

Mach number 2, with a corresponding static pressure of 10,000 Pa and a density of 2.2 kg/m^3.

Measurements and calculations using the TUFF, GASP, and GIFS models were obtained with and without the injection stream. The simulations all assumed laminar flow. The measured, nondimensionalized pressure along the body surface without injection is compared with TUFF, GASP, and GIFS predictions in Fig. 15. Computational simulations involving injection are much more challenging because the transverse jet produces a region of three-dimensional separated flow. Whenever a secondary flow is injected into a supersonic primary stream, this flow acts as an obstacle and induces a strong bow shock on the upstream side of the injection point. This shock wave interacts with the boundary layer on the wall, and the pressure is propagated through the boundary layer upstream of the shock, producing a boundary-layer separation region. For the case including injection, Fig. 16 presents a comparison of the measured, nondimensionalized pressure along the body surface and the simulated

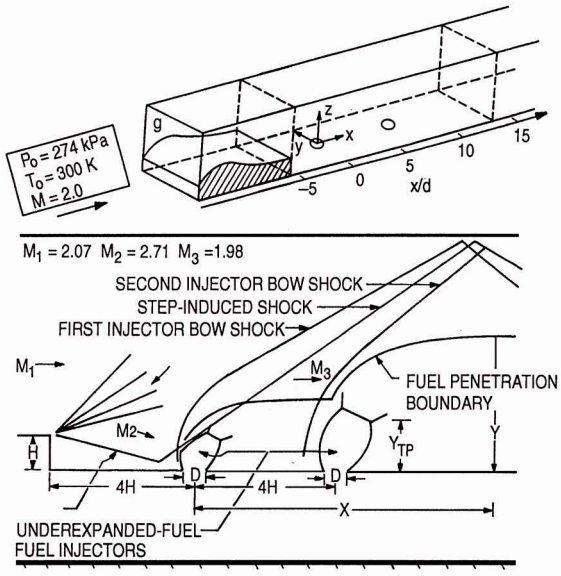

Fig. 17 Schematic of the staged transverse injection behind rearward-facing step.

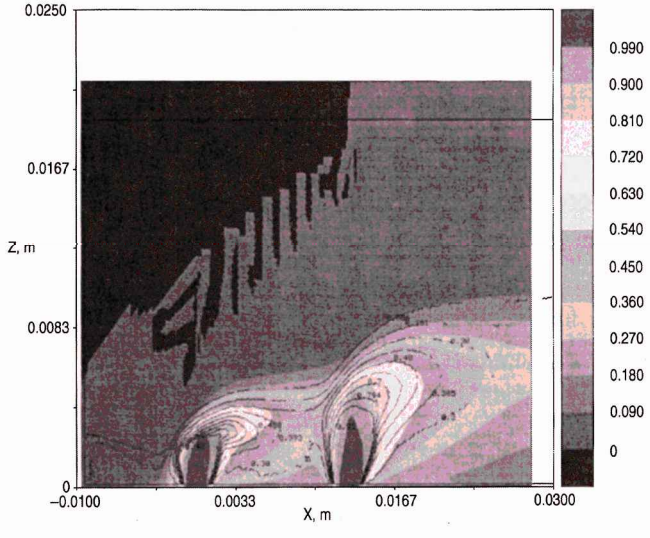

Fig. 18 Comparison of injectant mole fraction contours with experimental data (——).

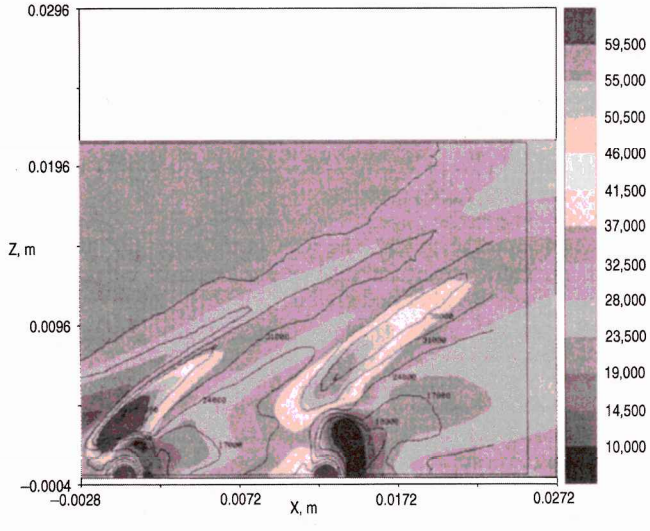

Fig. 19 Comparison of pressure contours with experimental data (——).

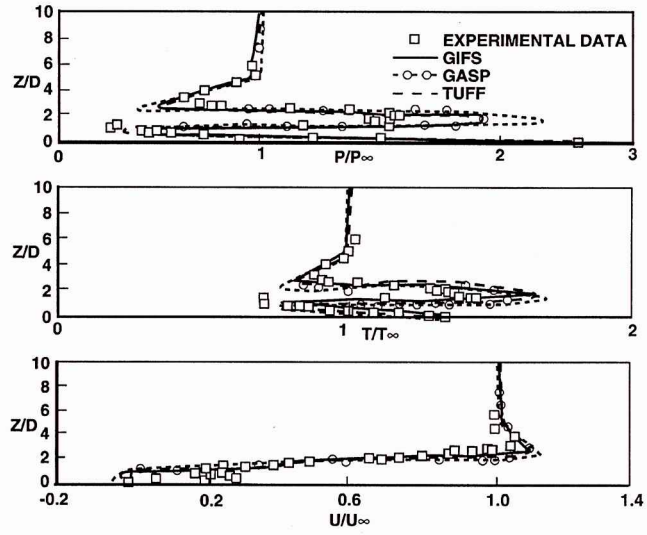

Fig. 20 Comparison of normalized flowfield profiles with data at $X/D = 0$.

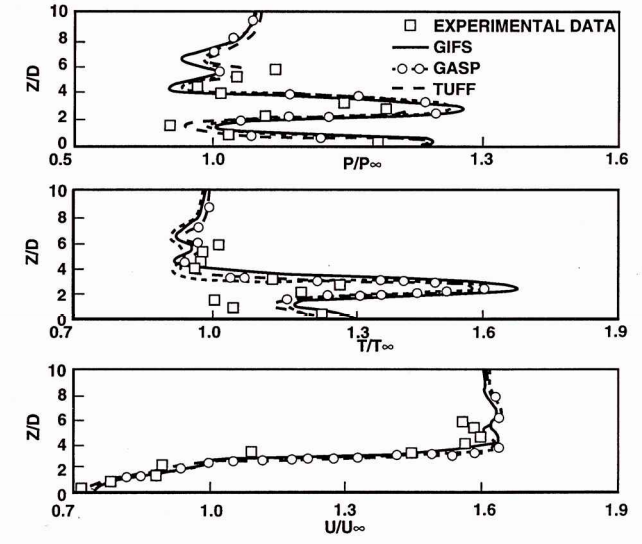

Fig. 21 Comparison of normalized flowfield profiles with data at $X/D_j = 6.6$.

pressures predicted by the GIFS, GASP, and TUFF models. It is apparent from Fig. 16 that the measured pressure rise attributed to the separation behind the bow shock is captured by all three CFD models, along with the measured pressure rise associated with the separation and the subsequent reattachment (or the recompression shock). Although the simulations all capture the expected initial pressure rise due to separation behind the bow shock, the experimental measurements do not show the initial pressure rise. This could be due to the failure to locate a pressure measurement port in the separation region.

Air–Air Staged Normal Injection

The staged normal injection of two N_2 jets located behind a rearward-facing step into a Mach 2 freestream airflow was investigated experimentally by McDaniel.[18] The geometry consists of a channel with a 3.18-mm step with two injectors of 1.93-mm diam positioned on the centerline at 3 and 7 step-heights downstream of the step. The height of the channel is 11.03 injector diameters, and it is 15.79 injector diameters wide. The main freestream flow conditions are specified by a stagnation temperature of 300 K and a stagnation pressure of 274 KPa. The flowfield geometry is shown schematically in Fig. 17. The computational grid consisted of 94 points in the streamwise direction, 61 points in the vertical direction, and 36 points in the lateral direction. Measured contours of static pressure and species mass fractions are compared with GIFS

predicted contours at the $y = 0$ plane in Figs. 18 and 19. The TUFF and GASP solutions produced results similar to the GIFS code; however, for clarity, they are not included in the figures. Comparisons of the experimental data and computed normalized axial velocity, static pressure, and static temperature profiles at the two injector locations are shown in Figs. 20 and 21. Qualitatively, the features of the calculated mass fractions, axial velocity, and static pressures are in reasonable agreement with the data. The computed and measured axial velocity contours in the regions behind the step and between the injectors are distinguished by recirculation zones, which appear to be smaller in magnitude than the experimental data indicate.

Summary

The application of a reliable CFD methodology in the design process of propulsion systems is a powerful and economic supplement to traditional cut-and-try design methods. The primary objectives of the work reported involved two efforts: selection of quality data sets appropriate to the validation of CFD models of propulsion flow phenomena and the comparison of the validation data sets with solutions obtained by CFD models, specifically, the GIFS, TUFF, and GASP computer programs. All three CFD models exhibited good agreement with the experimental data. However, due to long execution times, the evaluated version of the TUFF code is not feasible for engineering design purposes. Subsequent to this effort, an improved version of the TUFF model that claims improved execution times was released. The ultimate objective of the effort is to establish a standard validation database, including simple and complex experiments that can be used for the validation of CFD computer models in the subsonic through hypersonic flow regimes. In this way, CFD models can be directly compared and contrasted against a standard, baseline validation set.

Selected CFD computer models were examined to assess their capabilities to provide timely, efficient solutions and capture the primary flow physics associated with hypersonic flow regimes. These effects included chemical kinetics, three-dimensional flows, low subsonic to high supersonic flows, and turbulence.

A literature survey was conducted to identify experimental measurement programs with sufficient documentation of the geometry and flow conditions to model the experiment. Detailed measurements were extracted from the documents and archived, to establish a standard validation database. The selected experiments included simple flow environments and extended complex conditions representative of three-dimensional, chemically reacting, hypersonic combustor and nozzle flowfields. The experimental conditions included supersonic airflow over a rearward-facing step at Mach numbers 2.5 and 3.5; four supersonic nozzle configurations exhausting into a Mach number 6.0 freestream with air as the working fluid, a simulated scramjet combustor with tangential hydrogen injection into a Mach 2.44 airflow, an axisymmetric combustor configuration with hydrogen injection along the flow centerline, a biconic test model with perpendicular nitrogen injection into an air freestream, and staged transverse of N_2 injection into a Mach 2 airflow behind a rearward-facing step.

The importance and sensitivity of the assumed inflow property profile on the calculated downstream results were also demonstrated using the TUFF, GASP, and GIFS models. This continues to be an area of concern for modeling experimental conditions where the inflow conditions are not measured and are assumed to be one dimensional across the inflow plane. It was shown that more representative initial profiles result in improved comparisons with downstream data.

The results reported here indicate that the modified version of the GIFS CFD model is a viable approach for analyzing combustors and rocket-generated flowfields. The GIFS CPU execution time requirements generally were not as good as the GASP requirements. Also, the code architecture makes modifications and improvements in the GIFS model more difficult. This is due to the early development status of this version of the code. In contrast, the TUFF code was relatively easy to modify because the source is generously commented and a header was included at the top of each subroutine describing its function. The long CPU time requirements for this class of computer models remains an issue for design analysis; however, with appropriate initialization of the model, substantial reductions in the CPU time requirements can be realized.

The author has shown that all three CFD computer models can produce good results. However, GASP and GIFS have a variety of user options not available in the TUFF model. The GIFS code has a two-phase flow capability and a general chemistry model, which makes the code useful for solid rockets and aircraft icing. It has an CHIMERA capability, which enables simulations for bodies in relative motion. However, additional effort is required to modify the code to make it more robust and user friendly. The graphical user interface in GASP, version 3.0, is a useful tool for setting up problems. Its mesh sequencing option (converging a solution on a solution on a coarse mesh before interpolating to a finer mesh) is also very effective in reducing CPU time, especially in three-dimensional problems. The κ–ε model in GASP was not evaluated. This study has shown that the GASP code is computationally more efficient than the GIFS and TUFF codes.

Acknowledgments

Acknowledgment is given to D. W. Lankford, G. D. Ledbetter, R. L. Spinetti, and Martha A. Simmons for their valuable suggestions, technical support, and editing.

References

[1]Ebrahimi, H. B., "An Efficient Two-Dimensional Engineering Design Code for Scramjet Combustor, Nozzle, and Plume Analysis," AIAA Paper 91-0416, Jan. 1991.

[2]Ebrahimi, H. B., and Gilbertson, M., "Two- and Three-Dimensional Parabolized Navier–Stokes Code for Scramjet Combustor, Nozzle, and Film Cooling Analysis," AIAA Paper 92-0391, Jan. 1992.

[3]Ferri, A., "Review of Scramjet Propulsion Technology," *Journal of Aircraft*, Vol. 5, No. 1, 1978, pp. 3–10.

[4]Ebrahimi, H. B., "CFD Validation for Scramjet Combustor and Nozzle Flows, Part I," AIAA Paper 93-1840, June 1993.

[5]Ebrahimi, H. B., "CFD Validation and Evaluation for Combustor and Nozzle Flow, Part II," AIAA Paper 94-0025, Jan. 1994.

[6]Molvik, G. A., and Merkle, C., "A Set of Strongly Coupled Upwind Algorithms for Computing Flows in Chemical Non-Equilibrium," AIAA Paper 89-0199, Jan. 1989.

[7]Walters, W. R., Cinnella, D. C., and Halt, S. D., "Characteristic-Based Algorithms for Flows in Thermochemical Nonequilibrium," *AIAA Journal*, Vol. 30, No. 5, 1992, pp. 1304–1313.

[8]Holcomb, J. E., "Coupled Lewice/Navier–Stokes Code Development," AIAA Paper 91-0804, Jan. 1991.

[9]Ebrahimi, H. B., "Numerical Investigation of Multi-Plume Rocket Phenomenology," Workshop for CFD Applications in Rocket Propulsion, NASA Marshall Space Flight Center, Huntsville, AL, April 1996.

[10]Smith, H. E., "The Flow Field and Heat Transfer Downstream of a Rearward Facing Step in Supersonic Flow," U.S. Army Research Lab., ARL-67-0056, March 1967.

[11]Hopkins, H. B., Konopka, W., and Leng, J., "Validation of Scramjet Exhaust Simulation Technique at Mach 6," NASA CR 3003, April 1979.

[12]Kent, J. H., and Bilger, R. W., "Measurements in Turbulent Jet Diffusion Flames," Dept. of Mechanical Engineering, Rept. TNF-41, Univ. of Sydney, Sydney, Australia, Oct. 1972.

[13]Henry, J., and Beach, H. L., "Hypersonic Air Breathing Propulsion Systems," Paper 8, NASA SP-292, Nov. 1971.

[14]Burrows, M., and Kurkov, A. P., "Analytical and Experimental Study of Supersonic Combustion of Hydrogen in a Vitiated Airstream," NASA TMV-2828, Sept. 1973.

[15]Kamath, H., "Parabolized Navier–Stokes Algorithm for Chemically Reacting Flows," AIAA Paper 89-0386, Jan. 1989.

[16]Ebrahimi, H. B., "Parametric Investigation of the Effect of Various Phenomena on the Performance of a Scramjet Nozzle," AIAA Paper 95-6048, April 1995.

[17]Prats, B. D., Metzger, M. A., and Hill, J. A. F., "High-Altitude Maneuver Control Tests in the NSWC Hypervelocity Wind Tunnel," U.S. Naval Surface Weapons Center, NSWC MP 83-82, Silver Spring, MD, Jan. 1983.

[18]McDaniel, J. M., Fletcher, D., Hartfield, R., Jr., and Hollo, S., "Staged Transverse Injection into Mach 2 Flow Behind a Rearward Facing Step," AIAA Paper 91-5071, Dec. 1991.

T. C. Lin
Associate Editor